PNAS
www.pnas.org

Supplementary Information for

Pharmacokinetic modeling reveals parameters that govern tumor targeting and delivery by a pH-Low Insertion Peptide (pHLIP)

Alexander A. Svoronos, Donald M. Engelman*

***Corresponding author**
Email: donald.engelman@yale.edu

This PDF file includes:

Supplementary text
Model equations
Figures S1 to S8
Tables S1 to S3
SI References

Other supplementary materials for this manuscript include the following:

MATLAB code – downloadable from https://doi.org/10.5281/zenodo.4119903

1. Development of a Mathematical Model Describing pHLIP Transmembrane Insertion and Exit

To mathematically describe the State 2-State 3 equilibrium, we calculate pH-dependent rate constants for both transmembrane insertion and exit. The equilibrium can be described as the ratio between these rate constants, so we begin with the rate constant for the State 2 to State 3 transition in liposomes when the pH is dropped from 8 to 4, as measured previously in stopped-flow kinetic experiments (1-4). This rate constant can be interpreted as the maximum rate for transmembrane insertion (k_{23}^{max}), as nearly all pHLIP molecules would start in a deprotonated state at pH 8 and immediately become protonated, thereby initiating transmembrane insertion when the pH is dropped to 4. At intermediate pHs, there is a mix of protonated and deprotonated pHLIP molecules, and hence the rate constant for the State 2 to State 3 transition (k_{23}) can be estimated as the proportion of protonated pHLIP molecules multiplied by k_{23}^{max}. This proportion can be calculated from the Henderson-Hasselbalch equation with cooperativity, or Hill coefficient, resulting in the following:

$$k_{23} = k_{23}^{max} * \frac{10^{n_{Ins}*(pKa_{Ins}-pHe)}}{1+10^{n_{Ins}*(pKa_{Ins}-pHe)}}$$

where pKa_{Ins}, n_{Ins}, and *pHe* are the pKa of insertion, cooperativity (Hill) coefficient of insertion, and outside (extracellular) pH, respectively. The rate constant for transmembrane exit (k_{32}) can be determined in the same manner:

$$k_{32} = k_{32}^{max} * \frac{10^{n_{Ex}*(pKa_{Ex}-pHi)}}{1+10^{n_{Ex}*(pKa_{Ex}-pHi)}}$$

where pKa_{Ex}, n_{Ex}, and *pHi* are the exit pKa, exit cooperativity coefficient, and inside (intracellular) pH, respectively. Of note, we set $k_{32}^{max} = k_{23}^{max}$ in our model. While it has been reported that transmembrane exit occurs much more quickly than insertion when pHLIP with liposomes at pH 4 is rapidly increased to pH 8 (1), the mechanism for transmembrane exit observed in this experiment was likely very different from what occurs physiologically, at equilibrium, given that it seems to depend on rapid deprotonation of pHLIP residues residing within the membrane, as opposed to the protonation of pHLIP residues residing inside the liposome. The mechanism for transmembrane exit at equilibrium is likely equivalent or very similar to the reverse of transmembrane insertion. Since the equilibrium ratio of State 3 to State 2 equals k_{23}/k_{32}, we can generate predicted titration curves for the degree of transmembrane insertion (Fig. S1) with the following calculation:

$$State\ 3\ Fraction = \frac{\frac{k_{23}}{k_{32}}}{1+\left(\frac{k_{23}}{k_{32}}\right)}.$$

Of note, one potential criticism of this model is that it does not take into account the fact that a significant proportion of pHLIP may be located in an intermediate state within the membrane at a given pH. To address this, we generated a modified model that includes an intermediate state:

$$State\ 2 \leftrightarrow Intermediate \leftrightarrow State\ 3$$

with the following equations:

$$k_{2i} = k_{23}^{max} * \frac{10^{n_{Ins}*(pKa_{Ins}-pHe)}}{1+10^{n_{Ins}*(pKa_{Ins}-pHe)}}$$

$$k_{i2} = k_{i3} = k_{23}^{max} = k_{32}^{max}$$

$$k_{3i} = k_{32}^{max} * \frac{10^{n_{Ex}*(pKa_{Ex}-pHi)}}{1+10^{n_{Ex}*(pKa_{Ex}-pHi)}}$$

where k_{2i}, k_{i2}, k_{i3}, and k_{3i} are the rates of the State 2 → Intermediate, Intermediate → State 2, Intermediate → State 3, and State 3 → Intermediate state transitions, respectively. In the intermediate state, the tryptophan residues of pHLIP are likely to be buried within the membrane, and hence the tryptophan fluorescence measurements which constitute the published titration curves are likely more representative of the intermediate state in addition to State 3, rather than State 3 alone. When we generate a titration curve using this model and pKa_{Ins} = 5.82 and pKa_{Ex} = 6.34, we still obtain a curve with a pKa of ~6, consistent with experimental results (Fig. S1*B*). Importantly, this model predicts that, for cells, a negligible amount of pHLIP is present in the intermediate state (Fig. S1*C*), and therefore our first model, which only includes State 2 and State 3, produces essentially identical results to the model with intermediate state. Hence, for our pharmacokinetic model, we modeled the State 2 to State 3 transition without the intermediate state, as this eliminated the intermediate state transition rate constants from the model, which have unknown values.

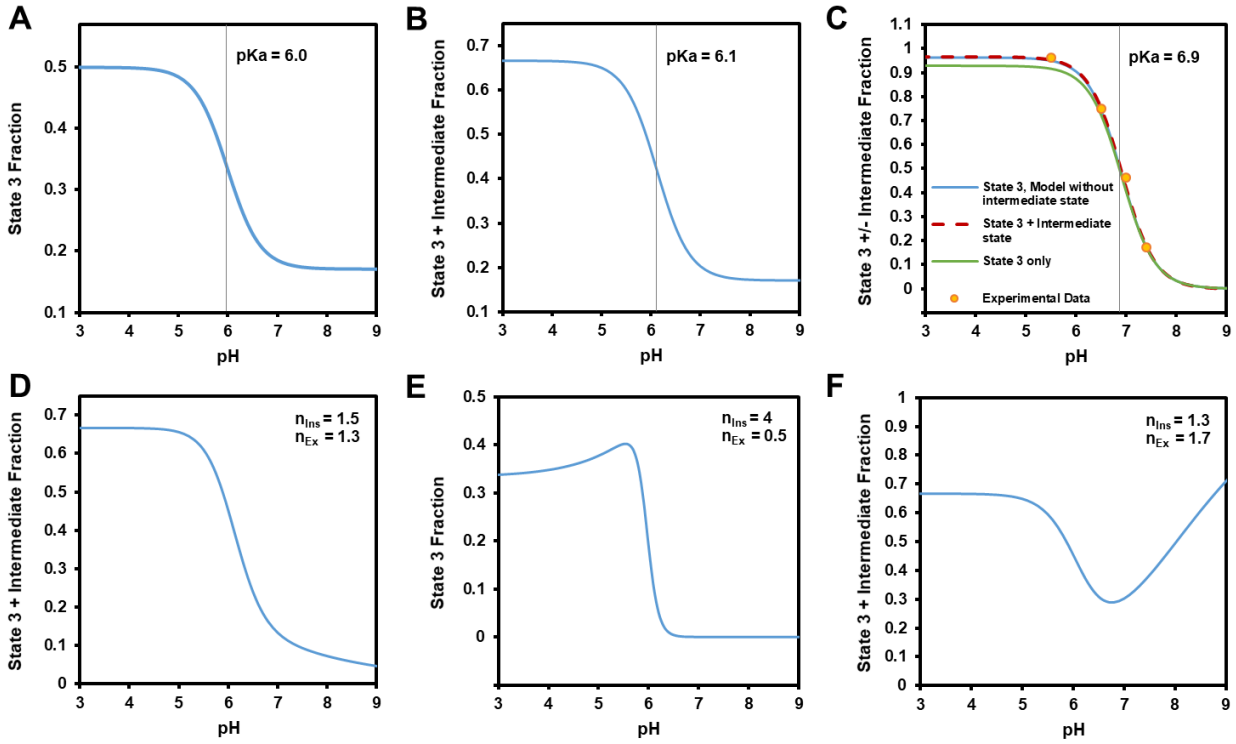

Fig. S1: pHLIP State 2-State 3 equilibrium titration curves predicted by the State 2 to State 3 transition model. Predicted titration curves for wildtype pHLIP insertion into POPC liposomes were generated using the model without intermediate state (*A*) and the model with intermediate state (*B*). Curves were also generated using both models for wildtype pHLIP insertion into cells (*C*). The predictions fit published experimental data from reference (5) (orange dots) well. For (*A*-*C*), $n_{Ins} = n_{Ex} = 1.32$. For curves (*D*-*F*), n_{Ins} and n_{Ex}, were varied. This altered the shape of the curves to include a "lagging tail" (*D*), an "upper hump" (*E*), and a reversal in trend (*F*).

Interestingly, when the cooperativity coefficients for insertion and exit, n_{Ins} and n_{Ex}, were varied, various features could be produced within the shape of the insertion titration curve for liposomes, many of which had been observed previously in published results. When $n_{Ins} = n_{Ex}$, the curve is symmetric (Fig. S1*A*,*B*). However, when n_{Ex} is slightly lower than n_{Ins}, a "lagging tail" feature is produced on the right side of the curve, indicating a reduced sharpness of transition for higher pHs (Fig. S1*D*). This feature appears

a number of times throughout the literature. In addition, when n_{Ins} is much greater than n_{Ex}, a hump is produced on the upper left of the curve (Fig. S1*E*). This feature appeared previously in the titration curve for pHLIP with N-terminally linked NBD, in which NBD fluorescence was measured instead of the standard tryptophan fluorescence (3). Notably, this curve had a very high cooperativity coefficient of 4.65, which is consistent with a very high n_{Ins} and comparatively low n_{Ex}. On the other hand, when $n_{Ins} < n_{Ex}$, the curve can exhibit a reversal in trend at higher pH values, in which the % State 3 increases with increasing pH (Fig. S1*F*). However, this (along with $pKa_{Ins} > pKa_{Ex}$) is unlikely to occur for any real pHLIP peptide or variant of pHLIP, since transmembrane exit is dependent on the protonation of a subset of the residues which are required to be protonated for transmembrane insertion. Of note, these features are only predicted to appear in the titration curves for liposomes; they do not appear when the same cooperativity coefficient values are applied to cells.

2. Pharmacokinetic Model Parameters

Table S1. Pharmacokinetic Model Parameters

Parameter	Default Value	Description	Source
pH Values			
pHe_{Tumor}	6.6	tumor extracellular pH	(6, 7)
pHi_{Tumor}	7.4	tumor intracellular pH	(8-10)
pHe_{Normal}	7.35	normal tissue extracellular pH	
pHi_{Normal}	7.2	normal tissue intracellular pH	
pHe_{Blood}	7.4	blood extracellular pH	
pHi_{Blood}	7.2	blood intracellular pH	
pHLIP Insertion Parameters			
pKa_{Ins}	5.82	pKa of pHLIP transmembrane insertion	(11)
pKa_{Ex}	6.34	pKa of pHLIP transmembrane exit	(11)
n_{Ins}	1.32	cooperativity coefficient for pHLIP insertion	Fitting State 2-State 3 equilibrium model to data from (5)
n_{Ex}	1.32	cooperativity coefficient for pHLIP exit	Fitting State 2-State 3 equilibrium model to data from (5)
EPR Effect			
EPRPermeabilityFactor	3.5	Tumor tissue permeability relative to normal tissue	Fitting model to data from (12)
EPRRetentionFactor	1.2	Tumor tissue retention relative to normal tissue	Fitting model to data from (12)

Volumes			
V_{Blood}	2	(mL) - total blood volume	
Hematocrit	45	(%) - hematocrit	
V_{Tumor}	1	(mL) - total tumor volume	
TumorIFFraction	0.3	Fraction of tumor consisting of interstitial fluid	(13, 14)
TumorBloodFraction	0.05	Fraction of tumor consisting of blood	(13)
$V_{NormalIF}$	4	(mL) - normal tissue interstitial fluid volume	
$V_{NormalCell}$	15.6	(mL) - normal tissue total cell volume	
Blood/Interstitial Fluid Partitioning			
f_{free}	0.5766	Free (unbound) pHLIP fraction	Measured
f_{prot}	0.3144	Protein-bound pHLIP fraction	Measured
f_{cell}	0.1089	Cell-bound pHLIP fraction	Measured
Rate Constants			
k_{23}	136.6	(hr^{-1}) - max rate of pHLIP transmembrane insertion (transition from State 2 to 3)	Overall rate constant calculated from 37°C data in (1)
k_{32}	136.6	(hr^{-1}) - max rate of pHLIP transmembrane exit (transition from State 3 to State 2)	Set equal to k_{23}
k_{EBF}	0.2086	(hr^{-1}) - rate of free pHLIP elimination from blood (e.g. by kidney clearance)	Derived from k_{EBP} and data in (7)
k_{EBP}	0.0945	(hr^{-1}) - rate of protein-bound pHLIP elimination from blood (e.g. by liver clearance)	Derived from data in (12)
k_E	0.006	(hr^{-1}) - rate of elimination of pHLIP that is bound to cells (e.g. by endolysosomal degradation)	(15)
k_{FBN}	1.777	(hr^{-1}) - rate of free pHLIP permeation from blood into normal tissue	Derived from k_{PBN} and data in (7)
k_{FNB}	0.2221	(hr^{-1}) - rate of free pHLIP permeation from normal tissue into blood	Derived from k_{PNB} and data in (7)
k_{PBN}	0.5575	(hr^{-1}) - rate of protein-bound pHLIP permeation from blood into normal tissue	Derived from data in (12)
k_{PNB}	0.8331	(hr^{-1}) - rate of protein-bound pHLIP permeation from normal tissue into blood	Derived from data in (12)

3. Pharmacokinetic Model Equations

3.1 Calculation of Blood Volumes, Tumor Volumes, and pHLIP Partitioning Rate Constants

Red Blood Cell Volume (mL): $V_{RBC} = V_{Blood} * \frac{Hematocrit}{100}$

Plasma Volume (mL): $V_{Plasma} = V_{Blood} - V_{RBC}$

Tumor Interstitial Fluid Volume (mL): $V_{TumorIF} = V_{Tumor} * TumorIFFraction$

Tumor Total Cell Volume (mL):

$$V_{TumorCell} = V_{Tumor} * (1 - TumorIFFraction - TumorBloodFraction)$$

Rate of pHLIP Protein Binding (hr^{-1}): $k_{FP} = \frac{f_{prot}}{f_{free}} * 1000$

Rate of pHLIP Protein Unbinding (hr^{-1}): $k_{PF} = 1000$

Rate of pHLIP Cell Membrane Binding (Transition from State 1 to 2) (hr^{-1}): $k_{F2} = \frac{f_{cell}}{f_{free}} * 1000$

Rate of pHLIP Cell Membrane Unbinding (Transition from State 2 to 1) (hr^{-1}): $k_{2F} = 1000$

3.2 Calculation of Parameter Values for Transfer between Blood and Tumor

Rate of free pHLIP permeation from blood into tumor (hr^{-1}): $k_{FBT} = k_{FBN} * \frac{0.98 * V_{Tumor}}{V_{NormalIF} + V_{NormalCell}}$

Rate of free pHLIP permeation from tumor into blood (hr^{-1}): $k_{FTB} = k_{FNB}$

Rate of protein-bound pHLIP permeation from blood into tumor (hr^{-1}):

$$k_{PBT} = EPRPermeabilityFactor * k_{PBN} * \frac{0.98 * V_{Tumor}}{V_{NormalIF} + V_{NormalCell}}$$

Rate of protein-bound pHLIP permeation from tumor into blood (hr^{-1}):

$$k_{PTB} = \frac{k_{PNB}}{EPRRetentionFactor}$$

3.3 Calculation of pH-Dependent Parameter Values

pHLIP State 2 to State 3 Transition Rate in Tumors (hr^{-1}): $k_{23}^{Tumor} = k_{23} * \frac{10^{n_{Ins}*(pKa_{Ins}-pHe_{Tumor})}}{1+10^{n_{Ins}*(pKa_{Ins}-pHe_{Tumor})}}$

pHLIP State 3 to State 2 Transition Rate in Tumors (hr^{-1}): $k_{32}^{Tumor} = k_{32} * \frac{10^{n_{Ex}*(pKa_{Ex}-pHi_{Tumor})}}{1+10^{n_{Ex}*(pKa_{Ex}-pHi_{Tumor})}}$

pHLIP State 2 to State 3 Transition Rate in Normal Tissue (hr^{-1}):

$$k_{23}^{Normal} = k_{23} * \frac{10^{n_{Ins}*(pKa_{Ins}-pHe_{Normal})}}{1+10^{n_{Ins}*(pKa_{Ins}-pHe_{Normal})}}$$

pHLIP State 3 to State 2 Transition Rate in Normal Tissue (hr^{-1}):

$$k_{32}^{Normal} = k_{32} * \frac{10^{n_{Ex}*(pKa_{Ex}-pHi_{Normal})}}{1+10^{n_{Ex}*(pKa_{Ex}-pHi_{Normal})}}$$

pHLIP State 2 to State 3 Transition Rate in Blood (hr^{-1}): $k_{23}^{Blood} = k_{23} * \frac{10^{n_{Ins}*(pKa_{Ins}-pHe_{Blood})}}{1+10^{n_{Ins}*(pKa_{Ins}-pHe_{Blood})}}$

pHLIP State 3 to State 2 Transition Rate in Blood (hr^{-1}): $k_{32}^{Blood} = k_{32} * \frac{10^{n_{Ex}*(pKa_{Ex}-pHi_{Blood})}}{1+10^{n_{Ex}*(pKa_{Ex}-pHi_{Blood})}}$

3.4 Dynamic Modeling Equations

$$V_{Plasma} * \frac{dC_{Free}^{Plasma}}{dt} = k_{PF} * C_{Protein}^{Plasma} * V_{Plasma} - k_{FP} * C_{Free}^{Plasma} * V_{Plasma} + k_{2F} * C_{State2}^{RBC} * V_{RBC} - k_{F2} * C_{Free}^{Plasma} * V_{Plasma} + k_{FTB} * C_{Free}^{TumorIF} * V_{TumorIF} - k_{FBT} * C_{Free}^{Plasma} * V_{Plasma} + k_{FNB} * C_{Free}^{NormalIF} * V_{NormalIF} - k_{FBN} * C_{Free}^{Plasma} * V_{Plasma} - k_{EBF} * C_{Free}^{Plasma} * V_{Plasma}$$

$$V_{Plasma} * \frac{dC_{Protein}^{Plasma}}{dt} = k_{FP} * C_{Free}^{Plasma} * V_{Plasma} - k_{PF} * C_{Protein}^{Plasma} * V_{Plasma} - k_{PBT} * C_{Protein}^{Plasma} * V_{Plasma} + k_{PTB} * C_{Protein}^{TumorIF} * V_{TumorIF} - k_{PBN} * C_{Protein}^{Plasma} * V_{Plasma} + k_{PNB} * C_{Protein}^{NormalIF} * V_{NormalIF} - k_{EBP} * C_{Protein}^{Plasma} * V_{Plasma}$$

$$V_{RBC} * \frac{dC_{State2}^{RBC}}{dt} = k_{F2} * C_{Free}^{Plasma} * V_{Plasma} - k_{2F} * C_{State2}^{RBC} * V_{RBC} - k_{23B} * C_{State2}^{RBC} * V_{RBC} + k_{32B} * C_{State3}^{RBC} * V_{RBC}$$

$$V_{RBC} * \frac{dC_{State3}^{RBC}}{dt} = k_{23B} * C_{State2}^{RBC} * V_{RBC} - k_{32B} * C_{State3}^{RBC} * V_{RBC}$$

$$V_{TumorIF} * \frac{dC_{Free}^{TumorIF}}{dt} = k_{PF} * C_{Protein}^{TumorIF} * V_{TumorIF} - k_{FP} * C_{Free}^{TumorIF} * V_{TumorIF} + k_{2F} * C_{State2}^{TumorCell} * V_{TumorCell} - k_{F2} * C_{Free}^{TumorIF} * V_{TumorIF} - k_{FTB} * C_{Free}^{TumorIF} * V_{TumorIF} + k_{FBT} * C_{Free}^{Plasma} * V_{Plasma}$$

$$V_{TumorIF} * \frac{dC_{Protein}^{TumorIF}}{dt} = k_{FP} * C_{Free}^{TumorIF} * V_{TumorIF} - k_{PF} * C_{Protein}^{TumorIF} * V_{TumorIF} + k_{PBT} * C_{Protein}^{Plasma} * V_{Plasma} - k_{PTB} * C_{Protein}^{TumorIF} * V_{TumorIF}$$

$$V_{TumorCell} * \frac{dC_{State2}^{TumorCell}}{dt} = k_{F2} * C_{Free}^{TumorIF} * V_{TumorIF} - k_{2F} * C_{State2}^{TumorCell} * V_{TumorCell} - k_{23T} * C_{State2}^{TumorCell} * V_{TumorCell} + k_{32T} * C_{State3}^{TumorCell} * V_{TumorCell} - k_E * TumorCell_{State2} * V_{TumorCell}$$

$$V_{TumorCell} * \frac{dC_{State3}^{TumorCell}}{dt} = k_{23T} * C_{State2}^{TumorCell} * V_{TumorCell} - k_{32T} * C_{State3}^{TumorCell} * V_{TumorCell} - k_E * TumorCell_{State3} * V_{TumorCell}$$

$$V_{NormalIF} * \frac{dC_{Free}^{NormalIF}}{dt} = k_{PF} * C_{Protein}^{NormalIF} * V_{NormalIF} - k_{FP} * C_{Free}^{NormalIF} * V_{NormalIF} + k_{2F} * C_{State2}^{NormalCell} * V_{NormalCell} - k_{F2} * C_{Free}^{NormalIF} * V_{NormalIF} - k_{FNB} * C_{Free}^{NormalIF} * V_{NormalIF} + k_{FBN} * C_{Free}^{Plasma} * V_{Plasma}$$

$$V_{NormalIF} * \frac{dC_{Protein}^{NormalIF}}{dt} = k_{FP} * C_{Free}^{NormalIF} * V_{NormalIF} - k_{PF} * C_{Protein}^{NormalIF} * V_{NormalIF} + k_{PBN} * C_{Protein}^{Plasma} * V_{Plasma} - k_{PNB} * C_{Protein}^{NormalIF} * V_{NormalIF}$$

$$V_{NormalCell} * \frac{dC_{State2}^{NormalCell}}{dt} = k_{F2} * C_{Free}^{NormalIF} * V_{NormalIF} - k_{2F} * C_{State2}^{NormalCell} * V_{NormalCell} - k_{23N} * C_{State2}^{NormalCell} * V_{NormalCell} + k_{32N} * C_{State3}^{NormalCell} * V_{NormalCell} - k_E * NormalCell_{State2} * V_{NormalCell}$$

$$V_{NormalCell} * \frac{dC_{State3}^{NormalCell}}{dt} = k_{23N} * C_{State2}^{NormalCell} * V_{NormalCell} - k_{32N} * C_{State3}^{NormalCell} * V_{NormalCell} - k_E * NormalCell_{State3} * V_{NormalCell}$$

3.5 State Variables

$C_{Free}^{Plasma} =$ free concentration in plasma

$C_{Protein}^{Plasma} =$ protein bound concentration in plasma

$C_{State2}^{RBC} =$ State 2 concentration in RBC blood fraction

$C_{State3}^{RBC} =$ State 3 concentration in RBC blood fraction

$C_{Free}^{TumorIF} =$ free concentration in tumor interstitial fluid

$C_{Protein}^{TumorIF} =$ protein bound concentration in tumor interstitial fluid

$C_{State2}^{TumorCell} =$ State 2 concentration in tumor cell fraction

$C_{State3}^{TumorCell} =$ State 3 concentration in tumor cell fraction

$C_{Free}^{NormalIF} =$ free concentration in normal tissue interstitial fluid

$C_{Protein}^{NormalIF} =$ protein bound concentration in normal tissue interstitial fluid

$C_{State2}^{NormalCell} =$ State 2 concentration in normal tissue cell fraction

$C_{State3}^{NormalCell} =$ State 3 concentration in normal tissue cell fraction

3.6 Initial Conditions

To simulate an intravenous injection of 3 nmoles into a mouse (for an initial overall blood concentration of 1500 nM, given a 2 mL blood volume), all pHLIP was assumed to initially be in free solution (State 1, not bound to protein) in the blood plasma. Hence,

$$C_{Free}^{Plasma} = (1500\ \text{nM})/(1 - Hematocrit)\ .$$

Concentrations of pHLIP in all other compartments were set to zero.

4. Derivation of Model Parameter Values

When available, parameter values were taken directly from the literature. Otherwise, they were measured or derived using the following methods. The derivation of the default values of n_{Ins} and n_{Ex} is explained in the main text.

4.1 Measurement of pHLIP Partitioning Fractions

For our model, it was necessary to determine the fractional partitioning of pHLIP between free, protein-bound, and cell-bound states while in biological fluid such as blood. For measuring cell binding, we used a modified version of the blood partitioning assay for drugs described by Yu et al., which determines the fraction of a drug in whole blood that binds to red blood cells (RBCs) (16). Briefly, the plasma volume fraction of a stock of whole blood was determined by centrifuging an aliquot of the stock in order to separate the plasma fraction from the RBC fraction and then measuring the volume of the plasma supernatant. A known amount of fluorophore-labeled pHLIP was then spiked into a known volume of whole blood or a volume of plasma equal to that inside the whole blood sample ($V_{Plasma} = V_{Blood}$*Plasma Fraction). The resulting two samples were then incubated for a set period of time (ranging from 30 seconds to 2 hours) at 37°C. Afterward, they were centrifuged, and the resulting plasma fractions were collected. The relative pHLIP concentrations in each sample were determined by measuring the absorbance from the pHLIP-linked fluorophore using a Cary 100-Bio UV-vis spectrophotometer. The concentration of pHLIP bound to RBCs was calculated as the difference in pHLIP concentration between the two samples. The fraction of pHLIP bound to RBCs, f_{cell}, was hence given by: $f_{cell} = (C_1 - C_2)/C_1$, where C_1 was the pHLIP concentration in the plasma-only sample, and C_2 was the pHLIP concentration in the plasma fraction of the whole blood sample.

To determine the protein-bound fraction of pHLIP, we used two distinct methods, which produced results that were in excellent agreement with each other. First, we used a protein precipitation-based method involving the addition of a 2-to-1 volume of acetonitrile to a plasma sample with known pHLIP concentration and a matched blank (no pHLIP) plasma sample, respectively, followed by immediate vortexing for ~10 seconds and centrifugation at 10,000xg for 1 minute. This method results in >96% precipitation of proteins ((17); also validated by ourselves from measuring absorbance at 280 nm before and after the procedure), along with protein-bound pHLIP, while free pHLIP remains in solution. Afterward, an equal amount of pHLIP was spiked into the supernatant from the blank plasma sample, and the respective absorbance of each sample supernatant was measured and compared to determine the concentration of pHLIP in the experimental sample's supernatant. This concentration, multiplied by three to account for the 2:1 acetonitrile dilution, was taken as the concentration of free pHLIP in the original plasma sample. The concentration of protein-bound pHLIP was determined by subtraction from the total pHLIP concentration in the original sample. The fraction of pHLIP bound to protein, f_{p0}, was hence given by: $f_{p0} = (C_3 - C_4)/C_3$, where C_3 was the pHLIP concentration in the spiked supernatant of the matched blank sample, and C_4 was the pHLIP concentration in the supernatant of the plasma sample. Of note, f_{p0} is the protein-bound fraction in the absence of RBCs (i.e., if f_{cell} were zero). To determine the fraction bound to protein in whole blood, f_{prot}, the equation $f_{prot} = f_{p0}/(1- f_{cell})$ was used. The fraction of free (unbound) pHLIP in whole blood, f_{free}, was then determined using the equation $f_{free} = 1 - f_{prot} - f_{cell}$.

We found the results produced from the acetonitrile addition assay to be precise and highly repeatable, even when different vortexing times were used and different times after centrifugation were allowed to pass, indicating that the protein-bound pHLIP did not dissociate from the precipitated protein over time. Nevertheless, it is known that the addition of organic solvent to a drug-protein mixture can sometimes result in the release of drug from the protein due to the different solvent environment and the structural changes associated with protein denaturation. It was hence necessary to validate the results

from the acetonitrile addition assay by comparison to a different protein binding assay. For this purpose, we attempted equilibrium dialysis and ultrafiltration, which are the most commonly used methods for measuring drug protein binding (18). However, we found wildtype pHLIP to be incompatible with these methods due to high nonspecific binding to the dialysis/ultrafiltration membrane, which prevented the pHLIP from crossing the membrane. We therefore used an erythrocyte partition method, similar to what has previously been done by others (19). The erythrocyte partition method essentially involves comparing the fraction of pHLIP bound to RBCs in the presence of plasma proteins to the fraction bound to RBCs in the absence of plasma proteins. Since protein-bound pHLIP is not available for binding to the surfaces of RBCs, the fraction of pHLIP bound to RBCs is reduced by the presence of plasma proteins, and the degree of protein binding can be calculated from the magnitude of this reduction.

The erythrocyte partition method involved repeating the assay we performed for measuring pHLIP binding to RBCs in whole blood, except with Hank's Balanced Salt Solution (HBSS) in place of plasma. To prepare the HBSS-RBC mixture, we first centrifuged whole blood at 2000xg for 15 min. at 4°C to separate the plasma and RBC fractions. We then aspirated the plasma and rinsed the remaining RBCs three times with fresh HBSS, followed by the addition of a volume of HBSS equal to the volume of the original plasma solution. Care was taken to ensure that the resulting HBSS volume fraction was precisely equal to the original plasma volume fraction. A known amount of fluorophore-labeled pHLIP was then spiked into a known volume of HBSS-RBC mixture or a volume of HBSS alone (without RBCs) equal to the HBSS volume inside the HBSS-RBC mixture sample. The resulting two samples were then incubated for 10 minutes at 37°C. Afterward, they were centrifuged, and the resulting HBSS fractions were collected. The relative pHLIP concentrations in each sample were determined by measuring the absorbance, and the concentration of pHLIP bound to RBCs was calculated as the difference in pHLIP concentration between the two samples. The fraction of pHLIP bound to RBCs, f_{c0}, was hence given by: $f_{c0} = (C_5 - C_6)/C_5$, where C_5 was the pHLIP concentration in the HBSS-only sample, and C_6 was the pHLIP concentration in the HBSS fraction of the HBSS-RBC mixture sample. We then combined this result with our result for the fraction of pHLIP bound to RBCs in whole blood, f_{cell}, to determine the protein-bound fraction of pHLIP within the whole blood sample, f_{prot}, using the following equation: $f_{prot} = 1 - f_{cell}\left(1 + \frac{1-f_{c0}}{f_{c0}}\right)$. The fraction of free (unbound) pHLIP in whole blood, f_{free}, was then again determined using the equation $f_{free} = 1 - f_{prot} - f_{cell}$.

Using the above methods, we measured the blood partitioning fractions of 1 µM wildtype pHLIP labeled at the N-terminus with either Alexa Fluor 594 or Alexa Fluor 750, respectively. Of note, the relative partitioning should be independent of concentration for pHLIP concentrations within this range or lower, since the plasma protein concentration is far in excess, and the available surface area for cell membrane binding is very large. Importantly, the results obtained using the erythrocyte partition method were in excellent agreement with those obtained from the acetonitrile addition method (Table S2). The acetonitrile addition method was therefore validated for each of these pHLIP constructs. Still, given the abovementioned potential issues with this method, we emphasize that it should always be validated by comparison to another method, even when used for similar pHLIP constructs. Nevertheless, once validated, the acetonitrile addition method appears to be superior to the erythrocyte partition method, as it appears to offer significantly higher precision (lower standard deviation). Notably, with both methods, the partitioning fractions were very similar for Alexa594-pHLIP and Alexa750-pHLIP (Table S2).

To gain insight into the kinetics of pHLIP partitioning, we performed the acetonitrile addition assay along with the whole blood RBC-binding assay for various incubation times (ranging from 30 seconds to 2 hours) after the addition of Alexa594-pHLIP to plasma or whole blood. Of note, it was necessary to use a fast whole blood centrifugation protocol (10,000xg for 1 minute) for this, as the shorter time points could not be measured otherwise. We found that this centrifugation protocol produced equivalent results, with no detectable RBC lysis and equivalent serum protein concentrations, to the standard protocol (2,000xg for 15 minutes), hence validating this method.

Using the above, we found the pHLIP partitioning fractions to be equal for all incubation times tested (Fig. S2). Hence, the kinetics of pHLIP partitioning are fast, on the order of seconds or less. Since it was not feasible to measure partitioning at shorter time points than ~30 seconds, we analyzed how the kinetics of pHLIP partitioning affect the results of our pharmacokinetic model. We found that for all partitioning times on the order of several minutes or less (> ~10 hr^{-1}), the results of our model are identical (Fig. S3). Hence, the exact values of the partitioning rate constants used in our model are unimportant as long as they are set above a certain threshold, and the ratios of the respective rate constants are such that the steady-state equilibrium values they would produce in a stable system result in the appropriate partitioning fractions. We hence set the transition rates for protein-bound pHLIP to free pHLIP (k_{PF}) and cell-bound (State 2) pHLIP to free pHLIP (k_{2F}) both to 1000 hr^{-1}. In order to have our model yield the appropriate partitioning fractions, we set the opposite transition rates (free pHLIP to protein-bound pHLIP, k_{FP}, and free-pHLIP to State 2 pHLIP, k_{F2}) to the following:

$$k_{FP} = \frac{f_{prot}}{f_{free}} * 1000\ \mathrm{hr}^{-1} \quad ; \quad k_{F2} = \frac{f_{cell}}{f_{free}} * 1000\ \mathrm{hr}^{-1}.$$

Table S2: Partitioning of Fluorophore-Labeled pHLIP in Whole Blood

	% Free	% Protein-bound	% RBC-bound
Alexa594-pHLIP (acetonitrile addition method)	57.7 ± 1.2	31.4 ± 1.2	10.9 ± 0.7
Alexa594-pHLIP (erythrocyte partition method)	60.0 ± 8.7	29.1 ± 8.0	10.9 ± 0.7
Alexa750-pHLIP (acetonitrile addition method)	58.8 ± 1.6	32.0 ± 1.6	9.2 ± 2.9
Alexa750-pHLIP (erythrocyte partition method)	55.2 ± 13.7	35.6 ± 10.8	9.2 ± 2.9

* Values are mean ± standard deviation, n = 3

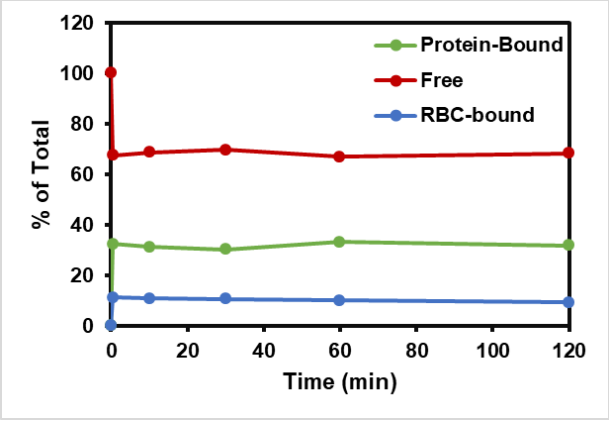

Fig. S2: Partitioning of pHLIP between free, protein-bound, and cell-bound fractions in whole blood after incubation times ranging from ~30 seconds to 2 hours.

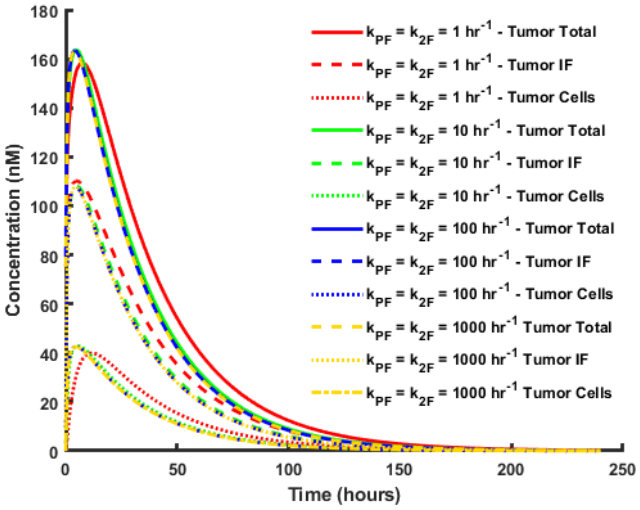

Fig. S3: Tumor concentration profiles produced by model for various pHLIP partitioning rates.

4.2 Derivation of Tissue-Blood Transport and Elimination Rate Constants

We derived the tissue-blood transport and elimination rate constants for pHLIP and mouse serum albumin from biodistribution data on their radiotracer-labeled counterparts, presented in references (7) and (12), respectively. This was done by fitting the respective blood concentration vs. time data to the biexponential decay curve typical of a drug after a single intravenous bolus (20):

$$C = A_1 e^{-\alpha t} + A_2 e^{-\beta t}$$

where *C* is the blood concentration, *t* is time, and A_1, A_2, α, and β are coefficients whose values are determined from the curve-fitting procedure. For a two-compartment model in which elimination primarily occurs through the central (blood) compartment, the elimination and blood-tissue transport rate constants can be calculated from the coefficients of the above equation as follows:

$$k_{21} = \frac{A_1\beta + A_2\alpha}{A_1 + A_2}$$

$$k_{el} = \frac{\alpha\beta}{k_{21}}$$

$$k_{12} = \alpha + \beta - k_{21} - k_{el}$$

where k_{21}, k_{12}, and k_{el} are the rate constants for tissue-to-blood transport, blood-to-tissue transport, and elimination from the blood compartment, respectively (20). Since the tumor compartment in our model is small relative to the normal tissue compartment, and elimination rates from the tissue compartments in our model are very low compared to elimination from the blood compartment, we could approximate our model as a two-compartment model and therefore use the above equations to calculate the respective elimination and blood ↔ normal tissue transport rate constants. We hence applied the above calculations to the fitted biexponential decay curves for pHLIP and mouse serum albumin, respectively, in order to determine the respective pHLIP and albumin rate constants.

Since the majority of serum protein consists of albumin, and pHLIP (~4 kDa) is significantly smaller than albumin (~66 kDa), we assumed protein-bound pHLIP to exhibit the same pharmacokinetics and hence have the same transport/elimination rate constants as albumin. We thus had rate constants for

total pHLIP (free + protein-bound + cell-bound) and protein-bound pHLIP. We assumed the transport and elimination rate constants to be zero for cell-bound pHLIP, since RBCs do not typically traverse through the lining of the vasculature and into interstitial fluid, and RBCs possess relatively long lifespans (~40 days in mice and ~120 days in humans). To calculate the rate constants for free pHLIP, we assumed the rate constants for total pHLIP to be the fraction-weighted averages of free, protein-bound, and cell-bound pHLIP. We hence used the following equation to solve for each free pHLIP rate constant, respectively: $k_{total} = f_{free} * k_{free} + f_{prot} * k_{prot} + f_{cell} * 0$, where k_{total}, k_{free}, and k_{prot} are the rate constants for total pHLIP, free pHLIP, and protein-bound pHLIP, respectively.

The transport rate constants calculated above were for transport between the blood and normal tissue compartments. The respective rate constants for blood-to-tumor transport were derived by assuming that blood flow to a compartment is directly proportional to the compartment's volume, and hence the blood-to-tumor rates were calculated as the blood-to-normal tissue rate constants multiplied by the ratio of tumor volume to normal tissue volume. For protein-bound pHLIP, the EPR effect was also accounted for by multiplying the blood-to-tumor rate constant by the *EPRPermeabilityFactor* and dividing the tumor-to-blood rate constant by the *EPRRetentionFactor*.

4.3 Derivation of Default *EPRPermeabilityFactor* and *EPRRetentionFactor* Values

To derive the default *EPRPermeabilityFactor* and *EPRRetentionFactor* values, we ran our model as if for an intravenous bolus of albumin as opposed to an intravenous bolus of pHLIP. To do this, we set the *ProteinFraction* in our model to 100% and ran it with the initial condition that $C_{Protein}^{Plasma} = (1500\ \mathrm{nM})/(1 - Hematocrit)$. Initial pHLIP concentrations in all other compartments were set to zero. Hence, 100% of pHLIP was in the protein-bound state throughout all time points in the model. We could therefore directly compare the model results with the experimental data on radiotracer-labeled albumin from reference (12). We ran the model over a range of *EPRPermeabilityFactor* and *EPRRetentionFactor* values and calculated the sum of the square differences in the contrast ratio produced from the model vs. the experimental data for each measured time point in the experimental data. These total square error values are graphically represented in Fig. S4. The *EPRPermeabilityFactor* and *EPRRetentionFactor* values which produced the minimum square error were taken to be the default values for our model.

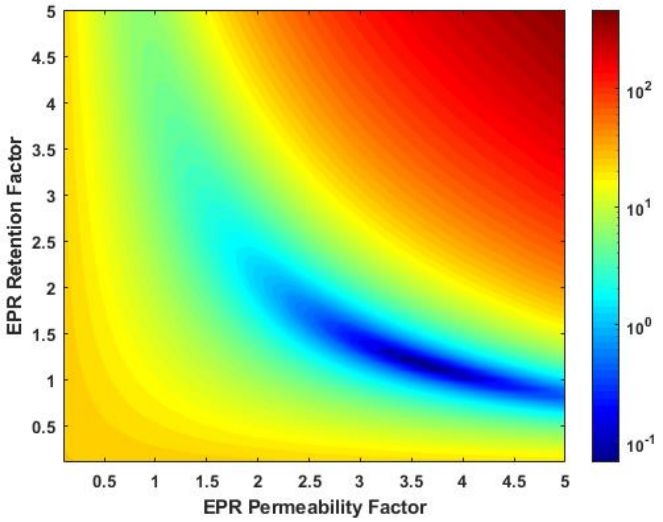

Fig. S4: Total square errors in contrast ratio produced between model and experimental data for *EPRPermeabilityFactor* and *EPRRetentionFactor* values ranging from 0.1 to 5.

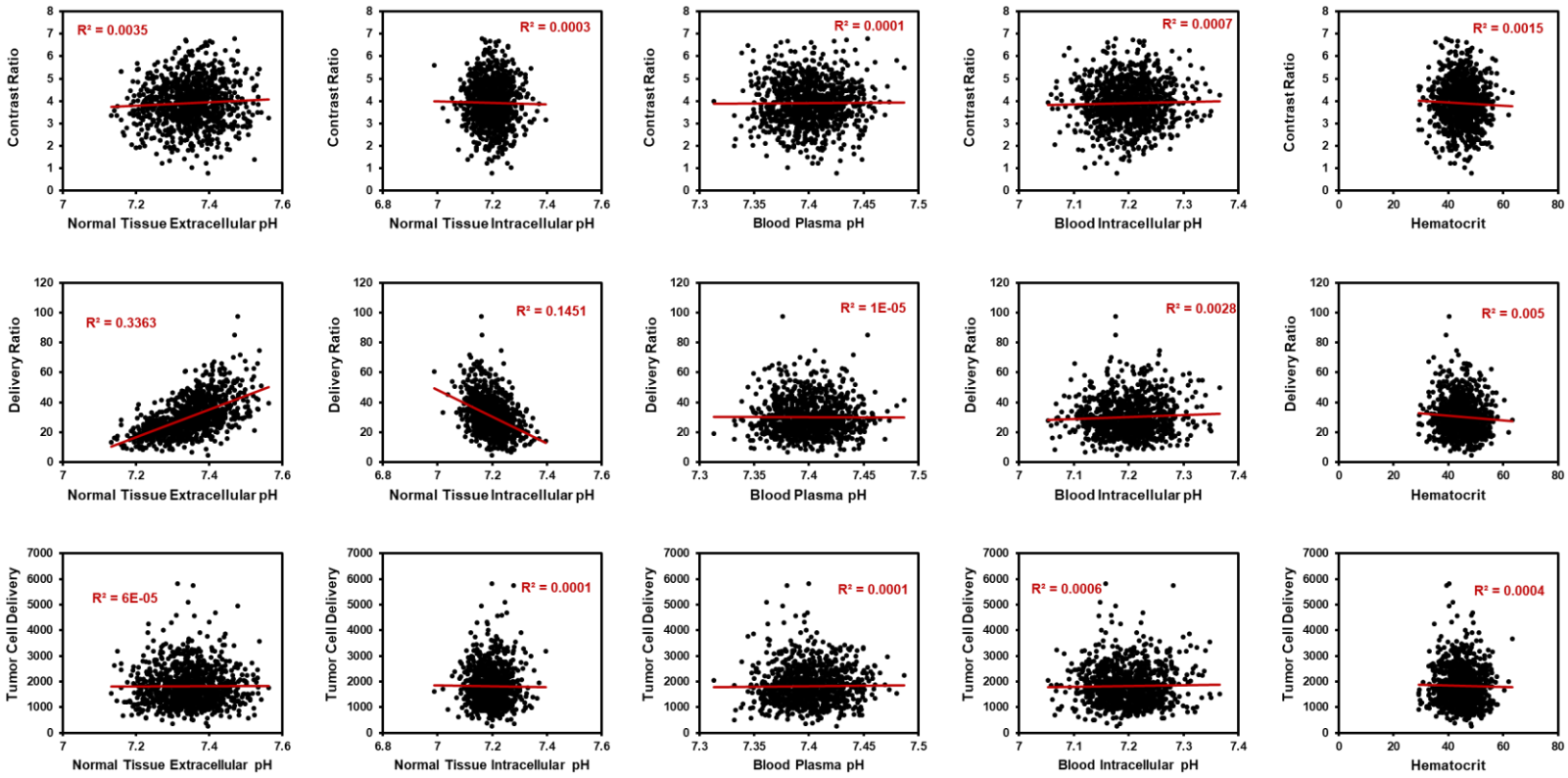

Fig. S5-1: Sensitivity Analysis of Biological Parameters. A sensitivity analysis was performed by running the model 1000 times with randomized biological parameters. The correlation between each parameter and the imaging contrast ratio (top), the delivery ratio (middle), and the magnitude of tumor cell delivery (bottom) are shown.

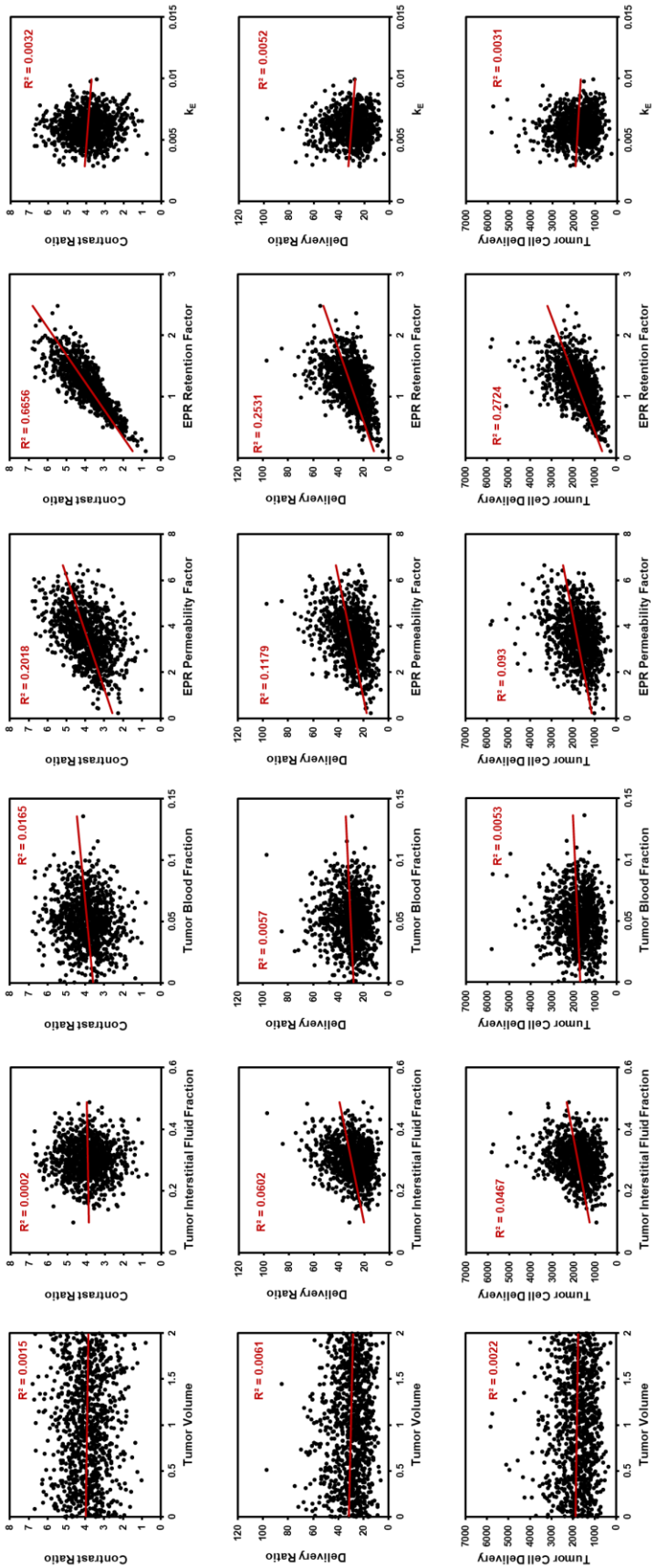

Fig. S5-2: Sensitivity Analysis of Biological Parameters (cont.).

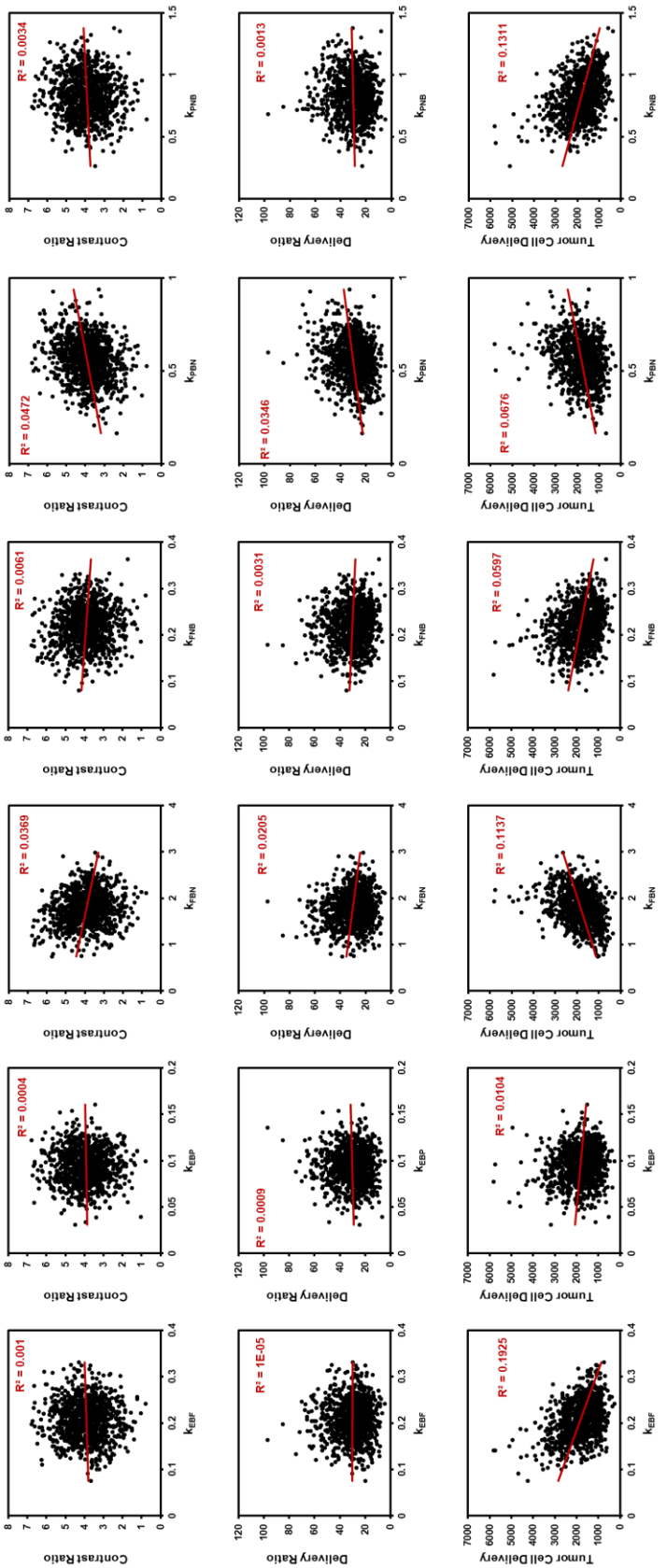

Fig. S5-3: Sensitivity Analysis of Biological Parameters (cont.).

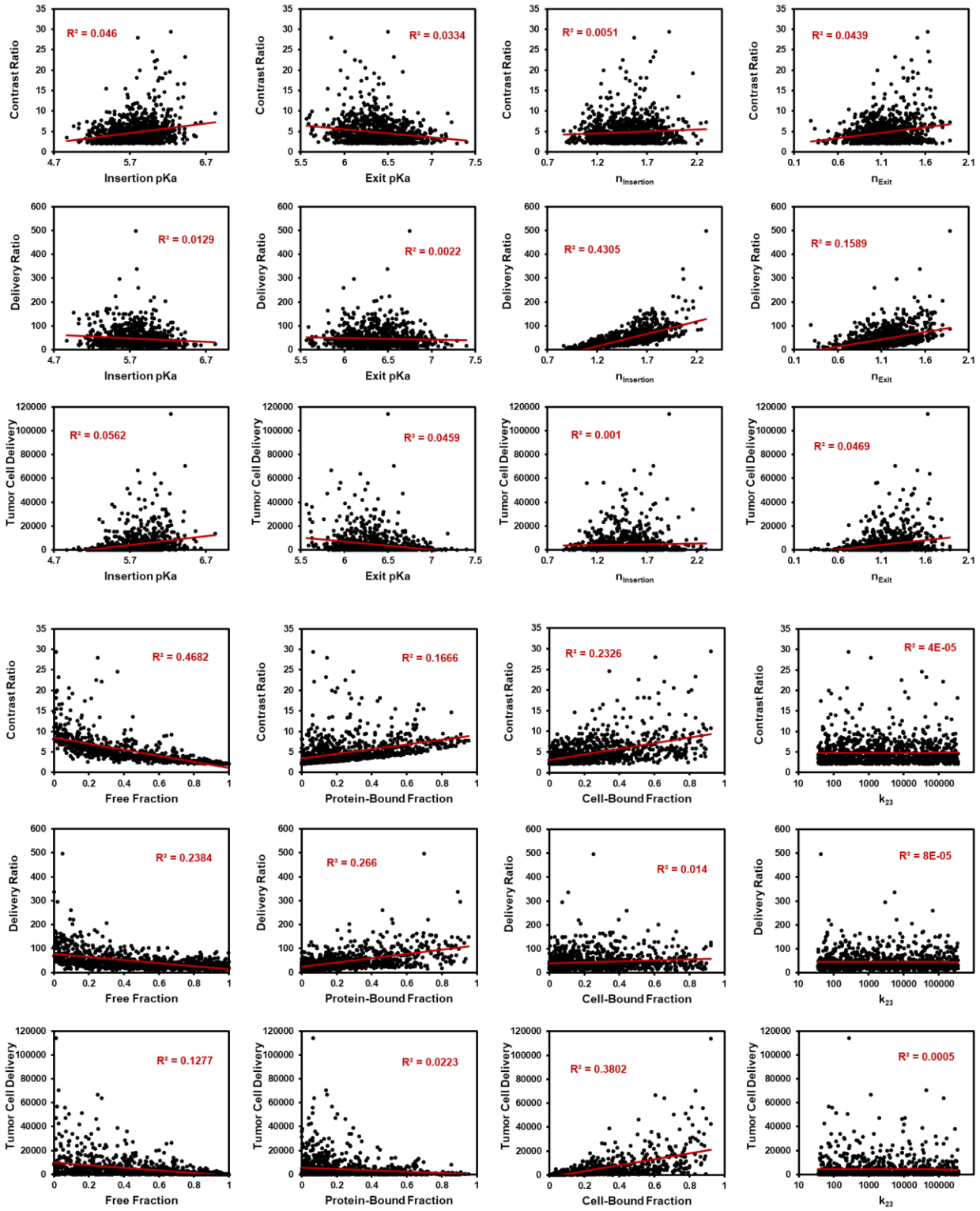

Fig. S6: Sensitivity Analysis of pHLIP Parameters. A sensitivity analysis was performed by running the model 1000 times with randomized pHLIP parameters. The correlation between each parameter and the imaging contrast ratio (top), the delivery ratio (middle), and the magnitude of tumor cell delivery (bottom) are shown.

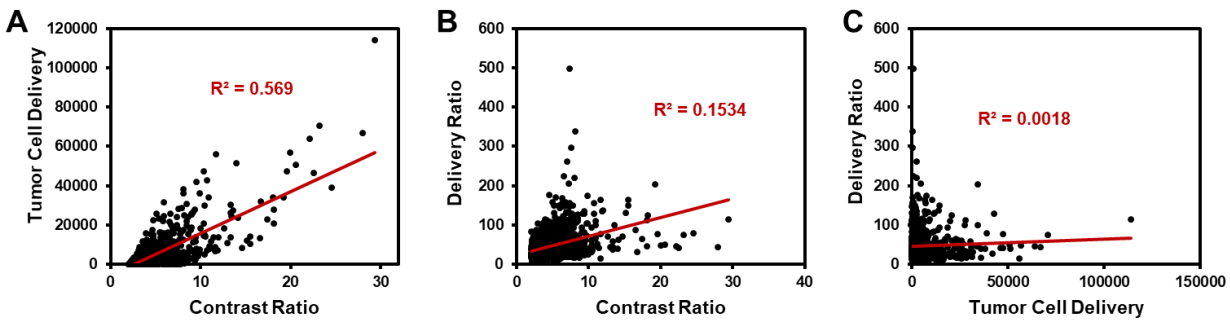

Fig. S7: Correlations between Targeting Ratios and Tumor Cell Delivery. The correlations between tumor cell delivery and imaging contrast ratio (*A*), delivery ratio and imaging contrast ratio (*B*), and delivery ratio and tumor cell delivery (*C*) are shown.

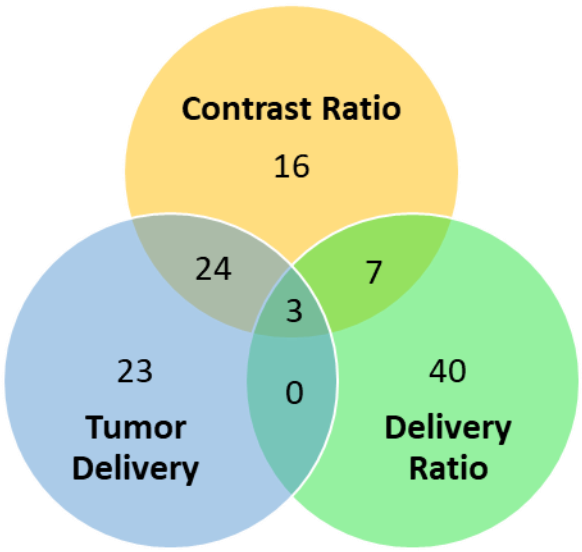

Fig. S8: Venn Diagram of Top Performing pHLIP Variants. The 50 highest performing pHLIP variants (top 5%) in terms of imaging contrast ratio, delivery ratio, and tumor cell delivery, respectively, were determined. Their distribution within each of these categories is shown. The intersections in the Venn diagram display the number of these pHLIP variants which were among the 50 highest performers in two or more categories.

Table S3: Properties of Top Performing pHLIP Variants.

	Contrast Ratio	Delivery Ratio	Relative Magnitude of Delivery	pKa_{Ins}	pKa_{Ex}	n_{Ins}	n_{Ex}	% Free	% Protein-Bound	% Cell-Bound
Wildtype pHLIP	3.95	29.5	1	5.82	6.34	1.32	1.32	57.7%	31.4%	10.9%
#1 Top Performer	29.4	114.0	66.2	6.24	6.50	1.92	1.63	1.2%	6.7%	92.1%
Top Delivery Ratio	7.3	497.1	0.29	5.78	6.75	2.29	1.89	4.9%	70.0%	25.1%
Top Performer with Equitable Partitioning	24.59	79.0	22.7	6.00	6.00	1.78	1.63	36.3%	29.3%	34.4%

SI References

1. Andreev OA, et al. (2010) pH (low) insertion peptide (pHLIP) inserts across a lipid bilayer as a helix and exits by a different path. Proceedings of the National Academy of Sciences of the United States of America 107(9):4081-4086.
2. Karabadzhak AG, et al. (2012) Modulation of the pHLIP transmembrane helix insertion pathway. Biophys J 102(8):1846-1855.
3. Scott HL, Westerfield JM, & Barrera FN (2017) Determination of the Membrane Translocation pK of the pH-Low Insertion Peptide. Biophys J 113(4):869-879.
4. Weerakkody D, et al. (2013) Family of pH (low) insertion peptides for tumor targeting. Proceedings of the National Academy of Sciences of the United States of America 110(15):5834-5839.
5. Reshetnyak YK, Andreev OA, Lehnert U, & Engelman DM (2006) Translocation of molecules into cells by pH-dependent insertion of a transmembrane helix. Proceedings of the National Academy of Sciences of the United States of America 103(17):6460-6465.
6. Macholl S, et al. (2012) In vivo pH imaging with (99m)Tc-pHLIP. Mol Imaging Biol 14(6):725-734.
7. Vavere AL, et al. (2009) A novel technology for the imaging of acidic prostate tumors by positron emission tomography. Cancer research 69(10):4510-4516.
8. Tafani M, et al. (2002) Regulation of Intracellular pH Mediates Bax Activation in HeLa Cells Treated with Staurosporine or Tumor Necrosis Factor-α. Journal of Biological Chemistry 277(51):49569-49576.
9. Webb BA, Chimenti M, Jacobson MP, & Barber DL (2011) Dysregulated pH: a perfect storm for cancer progression. Nature reviews. Cancer 11(9):671-677.
10. White KA, Grillo-Hill BK, & Barber DL (2017) Cancer cell behaviors mediated by dysregulated pH dynamics at a glance. Journal of Cell Science 130(4):663-669.
11. Hanz SZ, et al. (2016) Protonation-Driven Membrane Insertion of a pH-Low Insertion Peptide. Angewandte Chemie 55(40):12376-12381.
12. Heneweer C, Holland JP, Divilov V, Carlin S, & Lewis JS (2011) Magnitude of enhanced permeability and retention effect in tumors with different phenotypes: 89Zr-albumin as a model system. J Nucl Med 52(4):625-633.
13. Ballesta A, Zhou Q, Zhang X, Lv H, & Gallo JM (2014) Multiscale design of cell-type-specific pharmacokinetic/pharmacodynamic models for personalized medicine: application to temozolomide in brain tumors. CPT Pharmacometrics Syst Pharmacol 3:e112.
14. Kim YR, Savellano MD, Savellano DH, Weissleder R, & Bogdanov A (2004) Measurement of tumor interstitial volume fraction: Method and implication for drug delivery. Magn Reson Med 52(3):485-494.
15. Kaplan J & Moskowitz M (1975) Studies on the turnover of plasma membranes in cultured mammalina cells. I. Rates of synthesis and degradation of plasma membrane proteins and carbohydrates. Biochimica et biophysica acta 389(2):290-305.
16. Yu S, et al. (2005) A novel liquid chromatography/tandem mass spectrometry based depletion method for measuring red blood cell partitioning of pharmaceutical compounds in drug discovery. Rapid Commun Mass Spectrom 19(2):250-254.
17. Polson C, Sarkar P, Incledon B, Raguvaran V, & Grant R (2003) Optimization of protein precipitation based upon effectiveness of protein removal and ionization effect in liquid chromatography-tandem mass spectrometry. J Chromatogr B 785(2):263-275.
18. Bohnert T & Gan LS (2013) Plasma protein binding: from discovery to development. J Pharm Sci 102(9):2953-2994.
19. Trung AH, Sirois G, Dube LM, & McGilveray IJ (1984) Comparison of the erythrocyte partitioning method with two classical methods for estimating free drug fraction in plasma. Biopharm Drug Dispos 5(3):281-290.
20. Saltzman WM (2001) Drug delivery : engineering principles for drug therapy (Oxford University Press, Oxford England ; New York) pp xi, 372 p.